arXiv:1407.7797v2 [cond-mat.mes-hall] 8 Aug 2014

Metallic Surface States Probed Within the Microwave Skin Depth of the Putative Topological Insulator YBiPt Compound

G. G. Lesseux,[1] T. M. Garitezi,[1] P. F. S. Rosa,[1] C. B. R. Jesus,[1] R. R. Urbano,[1]
P. G. Pagliuso,[1] S. B. Oseroff,[2] J. L. Sarrao,[3] Z. Fisk,[4] and C. Rettori[1,5]

[1]*Instituto de Física "Gleb Wataghin", Universidade Estadual de Campinas, 13083-859, Campinas, SP, Brazil*
[2]*San Diego State University, 92182, San Diego, CA, USA*
[3]*Los Alamos National Laboratory, 87545, Los Alamos, NM, USA*
[4]*Department of Physics and Astronomy, University of California Irvine, 92697-4575, Irvine, CA, USA*
[5]*Centro de Ciências Naturais e Humanas, Universidade Federal do ABC, 09210-170, Santo André, SP, Brazil*

(Dated: August 11, 2014)

Electron Spin Resonance (ESR) experiments of diluted Nd^{3+} ions in the claimed topological insulator (TI) YBiPt are reported. Powdered samples with grain size from ≈ 100 μm to $\approx 2{,}000$ μm were investigated. At low temperatures, 1.6 K $\lesssim T \lesssim$ 20 K, the X-band (9.4 GHz) ESR spectra show a g-value of 2.66(4) and a Dysonian resonance lineshape which shows a remarkably unusual temperature, concentration, microwave power and particle size dependence. These results indicate that metallic and insulating behavior coexist within a skin depth of $\delta \approx 15$ μm. Furthermore, the Nd^{3+} spin dynamics in YBiPt are consistent with the existence of a *phonon-bottleneck process* which allows the energy absorbed by the Nd^{3+} ions at resonance to reach the thermal bath via the conduction electrons in the metallic surface states of YBiPt. These results are discussed in terms of the claimed topological semi-metal properties of YBiPt.

PACS numbers: 76.30.Kg, 76.30.-v, 73.20.At

I. INTRODUCTION

Topological insulator (TI) materials have recently attracted great attention of the condensed matter scientific community[1–3]. Nontrivial topological invariants of the bulk electronic band structure[4–6] yield a gapless state on the surface of these materials, which is protected by time-reversal symmetry. Examples of TI materials have been confirmed in quantum wells of HgTe/CdTe,[7,8] $Bi_{1-x}Sb_x$ alloys[9,10] and in the tetradymite semiconductors Bi_2Se_3, Bi_2Te_3, and Sb_2Te_3.[11–13] Besides these well established families of TI, several other classes of compounds have been recently proposed to be topological insulators, such as the Kondo insulator, SmB_6.[14–17]

In particular, the series of rare earth (RE) noncentrosymmetric half Heusler ternary semi-metallic compound, REBiPt, has been suggested by first principle calculations to host many three-dimensional topological insulators (3DTIs) owing to the fact that they have a topologically nontrivial band structure with band inversion which leads to a gap-less metallic surface.[18] In a 3DTI the bulk behaves as a small gap semiconductor ($\Delta \gtrsim 10$ meV) with robust protected metallic surface states due to their strong spin-orbit (SO) coupling and nontrivial Z_2 topology.[2,19]

Among the REBiPt compounds, YBiPt has gained distinguished attention due to its unusual transport properties which have been associated with the presence of surface states.[20] Moreover, superconductivity has been recently reported in YBiPt with a transition temperature at $T_c = 0.77$ K.[20] Superconductivity in noncentrosymmetric systems is an appropriated framework to study unconventional superconducting phases[21] due to their electronic band structure.[22,23] In addition, a superconducting phase in connection to non-trivial topology of the electronic bands may create propitious conditions to the investigation of surface states of Majorana fermions.[19,24]

However, superconductivity is not restricted to the claimed 3DTI YBiPt ($T_c = 0.77$ K)[20,25] within the REBiPt series. In fact, the metallic LuBiPt ($T_c = 1$ K)[26,27] and LaBiPt ($T_c = 0.9$ K)[28] compounds are also superconductor with similar critical temperatures.

Electron spin resonance (ESR) of diluted REs is a powerful local technique that can directly probe the localized magnetic moments and the nature of the interactions with their electronic environment.[29,30] Therefore, it may be an useful tool to investigate the dual character, metallic and insulating, of these TI materials.

In this regard, our group has studied the crystalline electric field (CEF) effects of diluted REs (Nd^{3+}, Gd^{3+} and Er^{3+}) in $Y_{1-x}RE_xBiPt$ about fifteen years ago.[31,32] At that time we found an intriguing behavior of the Nd^{3+} ESR lineshape in $Y_{1-x}Nd_xBiPt$ which we have chosen not to report so far because this result was disconnected from the study of CEF effects. Now, enlightened by the advent of the field of topological insulators and by the astonishing properties recently discovered in this material, we have revisited those data and performed further experiments in order to elucidate the origin of this unusual lineshape behavior. As such, here we report a detailed investigation of the Nd^{3+} ESR lineshape in $Y_{1-x}Nd_xBiPt$ and argue that our results provide important evidence for the existence of surface metallic states in YBiPt.

Our main ESR findings in $Y_{1-x}Nd_xBiPt$ ($0.002 \lesssim x \lesssim 0.10$) are: *i*) insulating and metallic behaviors coexisting within a microwave skin depth of $\delta \approx 15$ μm, which is considered a bulk measurement, even in normal metal-

lic systems;[29,30] *ii*) the ESR spectra depend on the microwave power, Nd^{3+} concentration, temperature and particle size; and *iii*) the existence of a *phonon-bottleneck* relaxation process in this TI. These features are discussed in terms of both phonons and Dirac conduction electrons (*ce*) contribution to the diffusion of the absorbed microwave energy at resonance by the Nd^{3+} ions to the thermal bath.

II. EXPERIMENTAL DETAILS

Several batches of $Y_{1-x}Nd_xBiPt$ ($0.002 \lesssim x \lesssim 0.10$) were synthesized using a self-flux technique[33] with a starting composition $(1-x)$Y:xNd:1Pt:20Bi. The crucible containing the elements was placed in a quartz tube sealed in vacuum and slowly heated up to 1170 ^{0}C. After being kept at this temperature for 2 h, the tube was cooled down to 900 ^{0}C with a rate of 10 ^{0}C/h. The collected crystals have free-growth planes with dimensions up to 4 mm. X-ray powder diffraction was used to verify the cubic crystal structure and F43m space group of YBiPt. The ESR experiments were performed on powdered single crystals of selected particles having sizes greater than 100 μm, corresponding to particles of average size/skin depth ratio, $\lambda = d/\delta \gtrsim 6.6$. The X-Band ($\nu \approx 9.4$ GHz) ESR experiments were carried out in a conventional CW Bruker-ELEXSYS 500 spectrometer using a TE_{102} cavity coupled to an Oxford helium gas flow system and a quartz/stainless steel cold tail liquid helium dewar.

III. EXPERIMENTAL RESULTS

First of all we will introduce the framework that will be necessary to analyze the ESR lineshape behavior in $Y_{1-x}Nd_xBiPt$. Due to the high conductivity of metals, the microwave electromagnetic field is attenuated and it only penetrates a small length scale called *skin depth* (δ). δ is frequently much smaller than the sample dimensions. It leads to a "vertically asymmetric" ESR lineshape named Dysonian (Fig. 1a).[34]

Furthermore, in a metal, a local moment spin system has a very fast relaxation process which allows the resonating spins to transfer the absorbed microwave energy to the lattice very rapidly via exchange interaction with the *ce*. As such, the ESR signal intensity (doubly integrated ESR spectrum) usually increases linearly as a function of the microwave power at a given temperature, as illustrated in Figure 1b.

In contrast, the microwave goes through the whole volume of an insulating material and the resonating spins present a symmetric ESR lineshape called Lorentzian as shown in Figure 1c. As the insulating materials are free of *ce*, the relaxation mechanism dominated by phonons is much slower than that of a metal. As a consequence, the ESR signal intensity in an insulator at a given temperature can saturate at high microwave power when the population of the spin levels, splitted by the Zeeman effect, tends to be equal. This effect is displayed in Figure 1d.

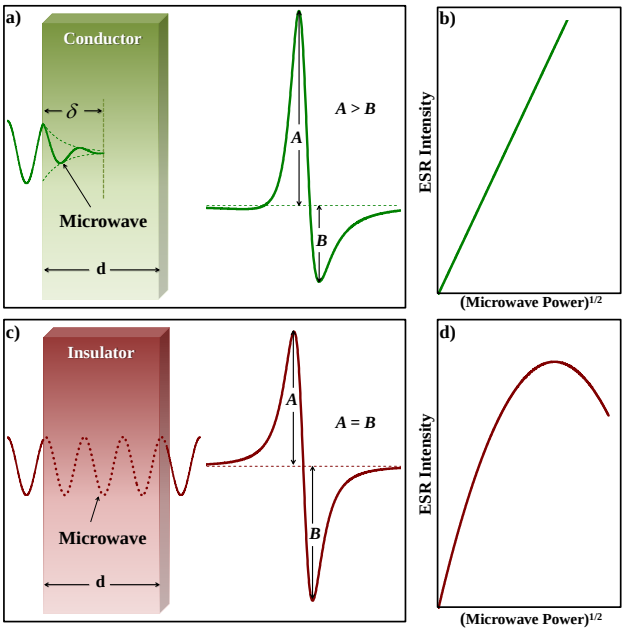

FIG. 1: (color online) a) and b) illustrate the microwave penetration and ESR lineshape; c) and d) the microwave power dependence of the ESR signal intensity in metallic and insulating samples, respectively.

In fact, the overall lineshape of the ESR spectra is analyzed by the general accepted approach where, at resonance, the microwave absorption in a metal is given by the Dyson theory in the diffusionless limit, $A/B \lesssim 2.6 \rightarrow T_D/T_2 \gg 1$[34,35]. In this limit, the Dyson theory can be approximated to a simple admixture of absorption and dispersion of Lorentzian lineshapes[36] with the A/B ratio changing monotonically from $A/B \approx 1$ to $A/B \approx 2.6$ for samples size, d, smaller and larger than δ, respectively[34–37]. However, when A/B exceeds 2.6 the Dyson theory anticipates the presence of diffusive effects, $A/B \gtrsim 2.6 \rightarrow T_D/T_2 \lesssim 1$, (Ref. 34 and Fig. 7)[34,35]. This means that the resonating spins diffuse through the skin-depth with a diffusion time, T_D, comparable to the spin-spin relaxation time, T_2.

Equation 1 gives the derivative of the admixture of absorption (χ'') and dispersion (χ') of Lorentzian lineshapes.

$$\begin{aligned} \frac{d\left[(1-\alpha)\chi'' + \alpha\chi'\right]}{dH} &= \chi_0 H_0 \gamma^2 T_2^2 \left[\frac{2(1-\alpha)\,x}{(1+x^2+s)^2} \right. \\ &+ \left. \frac{\alpha\left(1-x^2+s\right)}{(1+x^2+s)^2} \right] \qquad (1) \\ x &= (H_0 - H)\,\gamma T_2 \end{aligned}$$

where H_0 and H are the resonance and the applied magnetic fields respectively, γ is the gyromagnetic ratio, T_2 is the spin-spin relaxation time, α is the admixture of absorption ($\alpha = 0$) and dispersion ($\alpha = 1$), and χ_0 is the paramagnetic contribution from the static susceptibility.

In order to understand our results we have introduced the saturation term $s = \gamma^2 H_1^2 T_1 T_2$ in our resonance lineshape analysis phenomenologically. H_1 is the strength of the microwave magnetic field and T_1 is the spin-lattice relaxation time.[38]

Figure 2 presents the ESR spectra of Nd^{3+} in $Y_{1-x}Nd_xBiPt$ for $x = 0.002$ as well as natural Gd^{3+} impurities at $T = 1.6$ K and microwave power of $P_{\mu\omega} \approx 5$ mW for $\lambda \gg 132$. By a simple glance at this spectrum one can easily observe the striking and unexpected result that the recorded ESR lineshape for Gd^{3+} is typically metallic (Dysonian) corresponding to the diffusionless regime ($A/B \approx 2.6 \rightarrow T_D/T_2 \gg 1$) while that of the $^{140}Nd^{3+}$ ($I = 0$) presents, paradoxically, a completely diffusive lineshape ($A/B \approx 5 \rightarrow T_D/T_2 \approx 0.4$)[34,35], although both REs are localized magnetic moments diluted in the same material. Also, except for their concentrations, both probes are under the same conditions of T, $P_{\mu\omega}$ and particles size much larger than the skin depth.

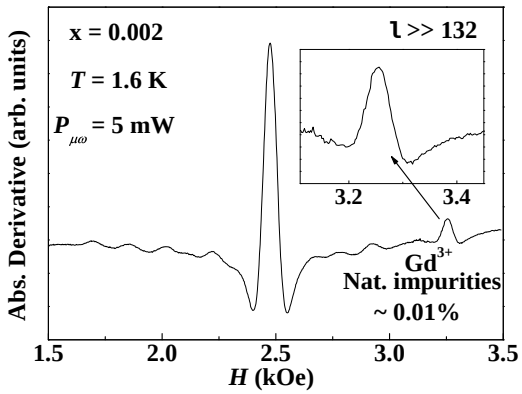

FIG. 2: ESR spectrum of $Y_{1-x}Nd_xBiPt$ for $x = 0.002$ and natural Gd^{3+} impurities at $T = 1.6$ K, $P_{\mu\omega} \approx 5$ mW and $\lambda \gg 132$. The inset shows the ESR lineshape for Gd^{3+}.

Figure 3a shows the ESR spectra of $Y_{1-x}Nd_xBiPt$ for $x = 0.10$ at $T = 4.2$ K and $P_{\mu\omega} \approx 8$ μW for $6.6 \lesssim \lambda \lesssim 132$. Remarkably, it is clear from these data that the observed change of the lineshape, going from $A/B \approx 3$ for large particles to $A/B \approx 7$ for smaller particles, does not correspond to the A/B values expected from the Dyson theory for diffusionless ESR lineshape ($1 \lesssim A/B \lesssim 2.6$). Instead, the lineshape of the smaller particles presents a strong diffusive shape, $A/B \approx 7 \rightarrow T_D/T_2 \approx 0.2$, despite the fact that the particles size is still larger than the skin depth. Figure 3b, in turn, presents the $P_{\mu\omega}$-dependence of the ESR lineshape for the $66 \lesssim \lambda \lesssim 132$ sample. These data show that at very low power (≈ 2 μW) the ESR lineshape is closer to the diffusionless limit ($A/B \approx 4 \rightarrow T_D/T_2 \approx 0.9$). However, by increasing $P_{\mu\omega}$ up to a power of ≈ 200 μW the lineshape becomes completely diffusive ($A/B \approx 14 \rightarrow T_D/T_2 \approx 0.02$). Yet, up to this power level the integrated ESR spectra grow linearly with $[P_{\mu\omega}]^{1/2}$ showing no saturation effects (not shown). Again, these results add up to contrasting behavior displayed by the ESR lineshape of localized magnetic moments in this material. By a further increasing $P_{\mu\omega}$, the lineshape remains diffusive and the double integrated spectra now display saturation effects (see Fig. 6b below).

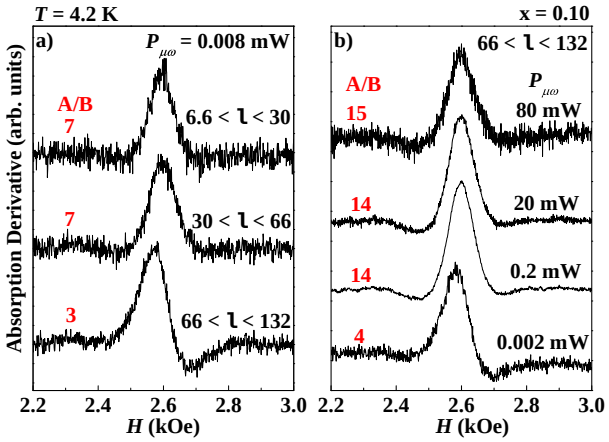

FIG. 3: (color online) a) Particle size dependence, $6.6 \lesssim \lambda \lesssim 132$, of the ESR spectra for $Y_{1-x}Nd_xBiPt$ ($x = 0.10$) at $T = 4.2$ K and $P_{\mu\omega} \approx 8$ μW. b) $P_{\mu\omega}$-dependence of the ESR lineshape for $Y_{1-x}Nd_xBiPt$ ($x = 0.10$) at $T = 4.2$ K and $66 \lesssim \lambda \lesssim 132$.

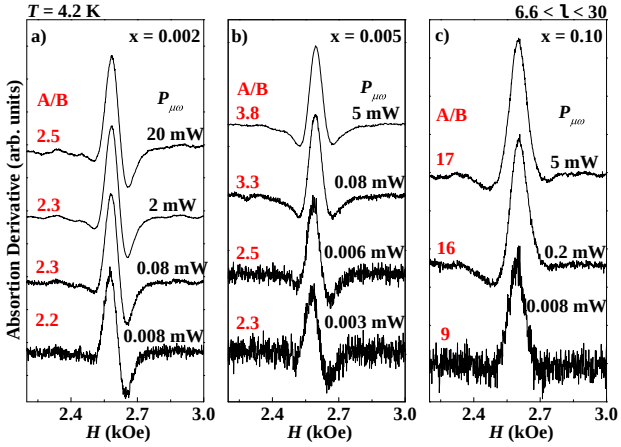

FIG. 4: $P_{\mu\omega}$-dependence of the ESR lineshape for $Y_{1-x}Nd_xBiPt$ at $T = 4.2$ K and $6.6 \lesssim \lambda \lesssim 30$ for: a) $x = 0.002$; b) $x = 0.005$; c) $x = 0.10$.

Figures 4a, 4b and 4c display the $P_{\mu\omega}$-dependence of the ESR lineshape of $Y_{1-x}Nd_xBiPt$ for $x = 0.002$, 0.005 and 0.10, respectively, at $T = 4.2$ K and $6.6 \lesssim \lambda \lesssim 30$. These results show that our smallest particles present almost diffusionless lineshapes ($A/B \approx 2.2$ - $2.5 \rightarrow T_D/T_2 \gg 1$) at low concentration and strong diffusive lineshapes ($A/B \approx 9$ - $17 \rightarrow T_D/T_2 \approx 0.10$ - 0.01) at high concentration, both nearly independent of $P_{\mu\omega}$. Nonetheless, for the intermediate concentration of $x = 0.005$ (Fig. 4b),

the lineshape presents a dramatic and unusual change between these two regimes, similarly to the data of Fig. 3b. This sample at $P_{\mu\omega} \approx 3$ μW shows a diffusionless ESR lineshape (A/B $\approx 2.3 \rightarrow T_D/T_2 \gg 1$). But, upon increasing $P_{\mu\omega}$ up to an intermediate power of ≈ 80 μW the lineshape becomes noticeably more diffusive (A/B $\approx 3.3 \rightarrow T_D/T_2 \approx 0.9$). Yet, up to these power levels, the double integrated ESR spectra do not show saturation effects (not shown). By a further increasing $P_{\mu\omega}$ the lineshape remains diffusive and at higher power levels the double integrated spectra display saturation effects (not shown), similar to the data shown in Figs. 6a, 6b.

Figures 5a, 5b and 5c present the T-dependence of the ESR lineshape of $Y_{1-x}Nd_xBiPt$ with $6.6 \lesssim \lambda \lesssim 30$ for $x = 0.002$ at $P_{\mu\omega} \approx 5$ mW, $x = 0.005$ at $P_{\mu\omega} \approx 5$ mW and $x = 0.10$ at $P_{\mu\omega} \approx 0.2$ mW, respectively. These results show that at $T \lesssim 10$ K the ESR lineshape displays strong diffusive character. The increase of T tends to restore the ESR lineshape into the diffusionless regime (A/B $\approx$ 2-4) as observed at low-$P_{\mu\omega}$ for large particles (see Figs. 2a, 2b).

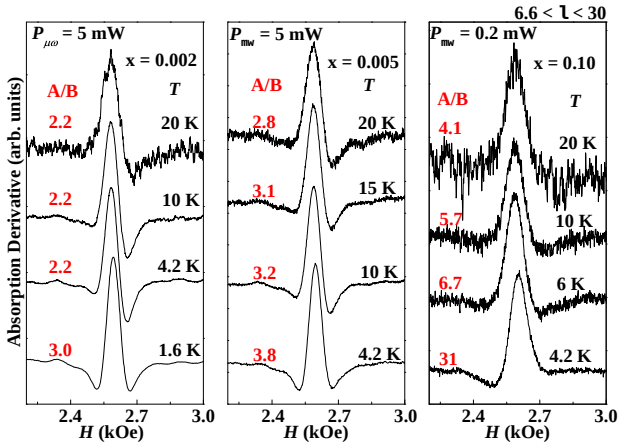

FIG. 5: (color online) T-dependence of the ESR lineshape for $Y_{1-x}Nd_xBiPt$ and $6.6 \lesssim \lambda \lesssim 30$; a) $x = 0.002$ at $P_{\mu\omega} \approx 5$ mW; b) $x = 0.005$ at $P_{\mu\omega} \approx 5$ mW; c) $x = 0.10$ at $P_{\mu\omega} \approx 0.2$ mW.

Figures 6a and 6b display the $P_{\mu\omega}$ and T-dependence of the double integrated ESR spectra of $Y_{1-x}Nd_xBiPt$ for $x = 0.002$ and 0.10, respectively, and $6.6 \lesssim \lambda \lesssim 30$. Similar results were obtained for the $x = 0.005$ and $x = 0.05$ samples (not shown). Strikingly, the saturation effects observed in the ESR spectra confirm that, as far as the relaxation processes are concerned, this system behaves as an insulator regardless the sample concentration. Therefore, we conclude that the ensemble of Nd^{3+} ions in the $Y_{1-x}Nd_xBiPt$ ($0.002 \lesssim x \lesssim 0.10$) system saturates as $P_{\mu\omega}$-increases and T-decreases. Notice that at high-T (8 K$\leq T \leq$ 20 K) the resonance intensity for the $x = 0.10$ sample saturates at relatively higher microwave power than that of the $x = 0.002$ sample. This is due to the large diffusive component of the ESR spectra for the $x = 0.10$ sample (see Fig. 5c). Figure 6c presents the x-dependence of the ESR spectra in $Y_{1-x}Nd_xBiPt$ ($0.002 \leq x \leq 0.10$) at 4.2 K and $P_{\mu\omega} \approx 5$ mW for $6.6 \lesssim \lambda \lesssim 30$. The best fit of the observed spectra to Eq. 1 using $1/T_2$ as a fit parameter is shown in red solid line. As expected for inhomogeneous ESR linewidths in insulators, the spin-spin relaxation rate, $1/T_2$, increases as x increases (see inset). Notice that a diffusive-like character of the lineshape is shown, though fortuitously, as x increases (A/B $\gg 2.6 \rightarrow T_D/T_2 \lesssim 1$).

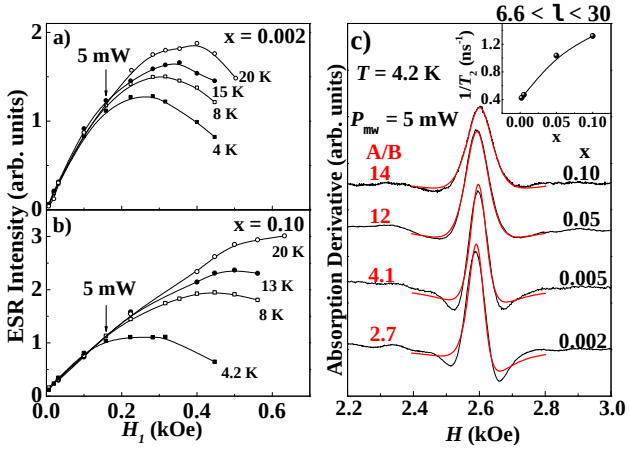

FIG. 6: (color online) $P_{\mu\omega}$ and T-dependence of the integrated ESR spectra for $Y_{1-x}Nd_xBiPt$ and $6.6 \lesssim \lambda \lesssim 30$ for: a) $x = 0.002$ and b) $x = 0.10$. The solid lines are guide to the eyes. c) x-dependence, $0.002 \lesssim x \lesssim 0.10$, of the ESR spectra for $Y_{1-x}Nd_xBiPt$ at $T = 4.2$ K, $P_{\mu\omega} \approx 5$ mW and $6.6 \lesssim \lambda \lesssim 30$. Red solid lines are the fits of the ESR spectra to Eq. 1 using $1/T_2$ as a fitting parameter. The inset shows the increase of $1/T_2$ as x increases. The solid line is a guide to the eyes.

Figure 7 shows the x-dependence of the spin-lattice relaxation rate, $1/T_1$, for $Y_{1-x}Nd_xBiPt$ at $T = 4.2$ K and $6.6 \lesssim \lambda \lesssim 30$. In the analysis of the various investigated samples, T_2 is obtained from the linewidth, $\Delta H = 1/\gamma T_2$, of the absorption component of the resonance at the lowest microwave power level. For T_1 it is only possible to estimate a lower limit (upper limit of $1/T_1$) from the saturation factor of the integrated ESR spectra, I_{sat}/I_{unsat}.[39] This limitation is due to the lack of an explicit equation which takes into account the ESR in the high microwave power regime for diffusive processes. Figure 7 shows that $1/T_1$ slows down as x increases indicating that in this system, as in other insulators, a *phonon-bottleneck process* dominates the spin-lattice relaxation as the Nd^{3+} concentration increases[40].

IV. ANALYSIS AND DISCUSSION

The Dysonian ESR lineshape of diluted Gd^{3+} and Nd^{3+} in YBiPt (Fig. 2) combined with the change of the Nd^{3+} ESR lineshape with the size of the powdered particles (Fig. 3a), assure us that these REs are probing the presence of *ce* within the skin depth of $\delta \approx 15$ μm. On the other hand, in our previous study on crystal

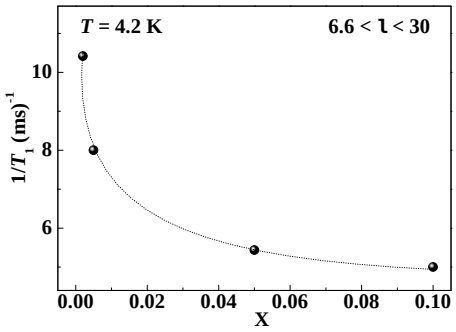

FIG. 7: x-dependence of $1/T_1$ for $Y_{1-x}Nd_xBiPt$ at $T = 4.2$ K and $6.6 \lesssim \lambda \lesssim 30$. The data was obtained from the analysis of the saturation factors[39] of the Nd^{3+} double integrated ESR spectra of various samples reported in this work. The dashed line is a guide to the eyes.

field effects of diluted REs (Nd^{3+}, Gd^{3+} and Er^{3+}) in $Y_{1-x}RE_xBiPt$ we have demonstrated that the exchange coupling between the RE localized magnetic moments and *ce* is very weak in this system.[31,32] This conclusion was drawn from the very small thermal broadening of the ESR linewidth (Korringa relaxation rates), the negligible g-shifts (Knight shifts) measured for these REs[41] and also corroborated by the small Sommerfeld coefficient ($\gamma \lesssim 0.1$ mJ/molK) found for this material.[32,42] These properties are consistent with the small gap ($\Delta \approx 0.1$ - 0.01 eV) reported for this semiconductor/semimetal YBiPt.[20,31–33] Therefore, as in any insulator in the diluted limit, the relaxation of the localized magnetic moments to the thermal bath should mainly happen through the lattice phonons via SO coupling ($\lambda_{4f}\boldsymbol{L}_{Nd}.\boldsymbol{S}_{Nd}$)[40] and not by the exchange interaction with *ce* ($(g_j\text{-}1)J_{fs}\boldsymbol{J}_{Nd}.\boldsymbol{s}_{ce}$)[41]. As such, in spite of the observed metallic ESR lineshapes of dysonian-like[34,35](see Figs 3, 4, 5 and 6), the low-T ESR linewidth of diluted REs in YBiPt is expected to be inhomogeneous (see Fig. 6c) and the spin-spin relaxation time much shorter than the spin-lattice relaxation time ($T_2 \ll T_1$) as in any insulator. Moreover, Figures 6a and 6b show that the double integrated Nd^{3+} ESR spectra saturates for $T \lesssim 20$ K and $P_{\mu\omega} \gtrsim 5$ mW, confirming the slow spin-lattice relaxation and indicating that the relaxation process is driven by phonons via SO coupling. This result combined with the dependence of the Nd^{3+} (Γ_6 Kramer doublet; $S_{eff} = 1/2$) ESR lineshape on the particle size (Fig. 2a), microwave power (Figs. 3b, 4a, 4b, 4c), temperature (Figs. 5a,b,c) and concentration (Fig. 6c) indubitably assure us that the insulating and metallic characters coexist in the YBiPt system.

Then, for the analysis of the ESR spectra we shall use Eq. 1 above. It is worth noting that one has to take our phenomenological lineshape analysis that uses the simple incorporation of the saturation term $s = \gamma^2 H_1^2 T_2 T_1$ into the admixture of absorption and dispersion with care. This may not completely describe the complex phenomenon involving the process of resonant microwave absorption diffusing to the thermal bath in the presence of a *phonon-bottleneck process* (see below).

Figure 8a shows the simulations of the data shown in Figs. 3b and 4b using Eq. 1. The spin-spin, $1/T_2$, and spin-lattice, $1/T_1$, relaxation rates were kept constant in these simulations. The simulated spectra show that the ESR lineshape changes as $P_{\mu\omega}$ increases, going from a diffusionless to a broad diffusive-like regime. Despite the broadening of the spectra, these simulations reproduce reasonably well the general lineshape features presented in Figs. 3b and 4b. Then, to avoid this broadening, not observed experimentally, we have forced the linewidth, $\Delta H = 1/\gamma T_2$, to narrow as $P_{\mu\omega}$ increases, holding $1/T_1$ constant. Figure 8b displays the simulated spectra for the ESR data of Fig. 4b. The inset shows the extracted phenomenological $P_{\mu\omega}$-dependence of $1/\gamma T_2$. Notice that the narrowing of the linewidth begins around $P_{\mu\omega} \approx 5$ mW where the resonance starts to saturate (*non-thermal equilibrium*) (see Figs. 6a, 6b). From this point on, an exponential behavior is obtained for the spin-spin relaxation rate, $1/T_2 \sim e^{-aP_{\mu\omega}}$, where a is a fitting parameter. The decrease of ΔH with $P_{\mu\omega}$ can be ascribed as a reduction of $1/T_2$ due to an evanescent local fluctuating field (*secular and non-secular broadenings*)[43], caused by the saturation of the ensemble of Nd^{3+} ions.

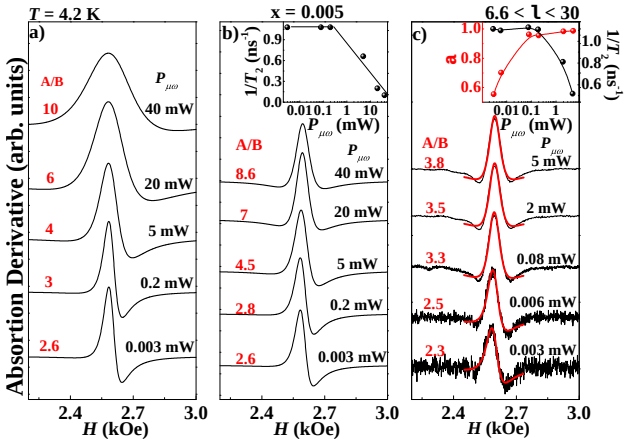

FIG. 8: (color online) Theoretical $P_{\mu\omega}$-dependence (Eq. 1) of the ESR lineshape for $Y_{1-x}Nd_xBiPt$ ($x = 0.005$) at $T = 4.2$ K and $6.6 \lesssim \lambda \lesssim 30$; a) simulations with constant relaxation rates, $1/T_2$ and $1/T_1$; b) simulations with $1/T_1$ constant and $1/T_2$ following the $P_{\mu\omega}$-dependence (logarithmic scale) shown in the inset and; c) the red lines are fits of the data of Fig. 4b with Eq.1 using constant $1/T_1$. The extracted parameters of absorption/dispersion admixture, α, and $1/T_2$ are shown in the inset. The solid lines are guide to the eyes.

Nonetheless, we believe that our most important and striking experimental result of the present work is the dramatic change of the Nd^{3+} ESR lineshape between the diffusionless (A/B ≈ 2.6; $T_D/T_2 \gg 1$) and diffusive regimes (A/B $\gtrsim 2.6 \rightarrow T_D/T_2 \lesssim 1$) observed for $P_{\mu\omega} \lesssim 200$ μW and $T \lesssim 10$ K. This change is clearly seen in the size (Fig. 3a), $P_{\mu\omega}$ (Figs. 3b and 4b) and T-dependence (Figs. 5a,b,c) of the ESR spectra.

For the $P_{\mu\omega}$-dependent case shown in Fig 4, the ESR

spectra display a drastic lineshape change well below ≈ 5 mW, the microwave power limit where saturation effects begin to be observed (Figs. 6a, 6b). Besides, this drastic lineshape change is revealed by our simulated spectra only at $P_{\mu\omega} \geq 20$ mW. For the samples of Figs. 3b and 4b this lineshape change occurs below ≈ 200 μW and ≈ 80 μW, respectively, (also for the sample with $x = 0.05$, not shown). Therefore, we conclude that the lineshape change for $P_{\mu\omega} \lesssim 200$ μW has nothing to do with the saturation phenomenon. Then, in Eq. 1 we again force the lineshape to change in the region of low-$P_{\mu\omega}$ adjusting the α parameter phenomenologically. Figure 8c presents, following the same procedure adopted for Figure 8b, the fits to the data of Figure 5b. It means that the admixture of absorption/dispersion (α in Eq. 1) was adjusted to fit the observed lineshape change to a pure diffusive regime ($T_D/T_2 \lesssim 1$). The extracted $P_{\mu\omega}$-dependence of α is shown in the inset of Figure 8c. Notice that the fits can not exactly reproduce the two minimum lateral of the resonances, although they show a change in the lineshape the same $P_{\mu\omega}$ (≈ 100 μW) as observed experimentally. This $P_{\mu\omega}$ is well below the regime where the saturation effects start to set in (≈ 5 mW). We believe that the inability of our fits to reproduce exactly the experimental spectra exactly may be due to the simplified phenomenological approach employed.

Regarding to the T-dependent ESR lineshape of Figure 5a, Figure 9 presents the fits of the spectra to Eq. 1. For these fits the spin-lattice relaxation rates, $1/T_1$, were estimated from the saturation factors[39] of Figure 6a (see inset of Fig. 9). Moreover, the T_2 and α parameters have been forced to assume the values that best fit the observed spectra. The obtained T-dependence of $1/T_2$, $1/T_1$ and α parameter are shown in the inset of Fig. 9. These results show that as T increases both $1/T_1$ and $1/T_2$ increase, restoring the local fluctuating field as the ensemble of Nd^{3+} ions reach their thermal equilibrium (unsaturated state). In other words, the phonon relaxation, via SO coupling, restore the local fluctuating field.

Now, based on the strong evidence displayed in Fig. 7 that the spin lattice relaxation of the Nd^{3+} ions is controlled by the *phonon-bottleneck phenomenon* in the high Nd^{3+} concentration limit, we conclude that the phonon-thermal bath contact must be poor and the Kapitza resistance[44] should be relatively high in YBiPt. Therefore, we suggest that the abrupt change of the lineshape, from diffusionless ($\alpha \approx 0.5 \rightarrow T_D/T_2 \gtrsim 1$) to diffusive ($\alpha \approx 1 \rightarrow T_D/T_2 \lesssim 1$), between ≈ 2 μW and ≈ 100 μW (Figs. 3b and 4b) and for $T \lesssim 10$ K (Figs. 5a, 5b, 5c), is associated to with the formation of a *long life time phonons reservoir* due to the poor phonon-thermal bath contact within the skin depth of $\delta \approx 15$ μm. Since the SO interaction ($\lambda_{ce}\boldsymbol{l}_{ce}.\boldsymbol{s}_{ce}$) is an important ingredient to form a TI[4–6] we argue that these *long life time phonons* could excite the *ce* in the metallic surface state of this TI compound via SO coupling. Which, in turn, deliver the microwave energy absorbed at resonance by the Nd^{3+} ions to the thermal bath. Then, this combination of *long life time phonons* and metallic surface states plays the role of *ce* diffusing across the skin depth in the usual Dyson theory for normal metals[35]. Figure 10 presents an illustrative route diagram indicating a plausible path (thick solid blue arrows) for the net flow of microwave energy absorbed at resonance reaching the thermal bath.

The intriguing results of Fig. 3a for $x = 0.10$ at low-$P_{\mu\omega}$ clearly show that a diffusionless lineshape occurs for the larger particles while for smaller ones a diffusive lineshape does. Such results can be also easily simulated (not shown) adjusting the α parameter in Eq. 1 as done for Figures 8c and 9. Notice that even for the smallest particles their size are several times larger than the skin depth. We believe that this remarkable lineshape change is due to the increase in the surface/volume ratio for the smaller particles which turns the *long life time phonons* interaction with the Dirac *ce* more effective. Therefore, smaller particles would favor the diffusion of the microwave energy absorbed at resonance by the Nd^{3+} ions to the thermal bath.

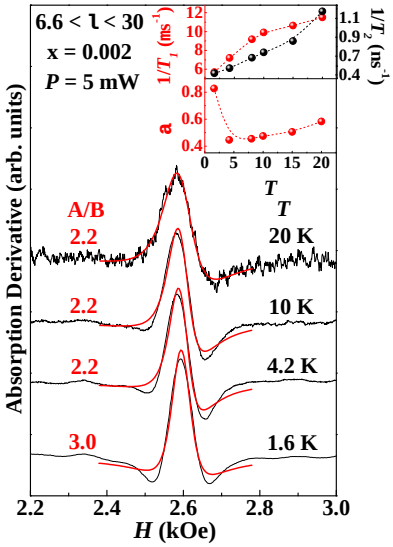

FIG. 9: (color online) The red lines are fittings to Eq. 1 of the T-dependence ESR lineshape for $Y_{1-x}Nd_xBiPt$ ($x = 0.002$) at $P_{\mu\omega} \approx 5$ mW and $6.6 \lesssim \lambda \lesssim 30$. For these fittings the spin-lattice relaxation rate, $1/T_1$, was obtained from the saturation data of Fig. 5a, the spin-spin relaxation rate, $1/T_2$, and α were free parameters that best fit the experimental spectra. Their T-dependence are shown in the inset. The dashed lines are guide to the eyes.

It is also worth mentioning that our microwave photons with energy $h\nu \simeq 0.5$ K may promote electrons across the gap of the Dirac cones, increasing the density of the *ce* on the surface as the microwave power increases. Thus, such an increase would favor the diffusion of the microwave energy absorbed at resonance by the Nd^{3+} ions to reach the thermal bath. This *ce* activation can be induced by electric dipolar transitions associated with the electric component of the applied microwave[45]. Nevertheless, this electronic activation may not be so relevant here because a TE_{102} ESR resonator was used in the ESR experiments.

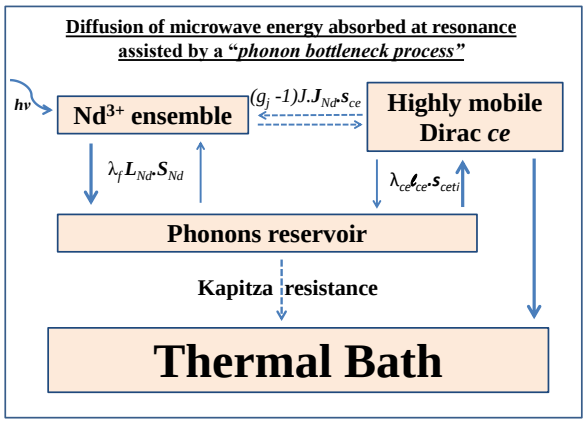

FIG. 10: (color online) Illustrative route diagram for the diffusion of the microwave energy absorbed at resonance to the thermal bath (thick solid blue arrows) assisted by the*phonon-bottleneck process*. The blue dashed arrows indicate week coupling mechanism.

This means that the sample is located at the minimum of the microwave electric field in the cavity.

Additionally, we should mention that we have carried out similar studies of Gd^{3+} in $Y_{1-x}Gd_xBiPt$ for $0.01 \lesssim x \lesssim 0.05$. Saturation effects at high microwave power, change of the ESR lineshape below ≈ 100 mW and *phonon-bottleneck effects*, similar to those of Nd^{3+} were also observed. However, describing the details of the Gd^{3+} ESR in YBiPt is beyond the scope of this work.

Finally, we believe that the results presented here will help to shed new light on the experimental characterization of the surface metallic states in TI materials. In particular, this work should motivate further ESR work in other TI materials. However, it is possible that the effects of the surface states would be favored to be observable by ESR in the presence of a *phonon-bottleneck* regime.

V. CONCLUSIONS

The systematic ESR study of the Nd^{3+} Γ_6 Kramer doublet ($S_{eff} = 1/2$) CEF ground state in the cubic noncentrosymmetric half Heusler semiconductor/semimetallic compound $Y_{1-x}Nd_xBiPt$ revealed that this system presents, simultaneously, metallic and insulating features. This dual character was verified by the saturation effects and relaxation processes observed on the Dysonian (metallic lineshape) of the Nd^{3+} ESR spectra. Also, our phenomenological approach to analyze the ESR lineshape suggests that saturation effects do affect the local fluctuation field and contribute to slow down the effective spin-spin relaxation rate, $1/T_2$, i.e., narrowing down the inhomogeneous ESR linewidth.

Moreover, the dramatic evolution of the lineshape between diffusionless ($A/B \lesssim 2.6 \rightarrow T_D/T_2 \gg 1$) and diffusive regimes ($A/B \gtrsim 2.6 \rightarrow T_D/T_2 \lesssim 1$) at microwave powers below ≈ 200 μW, where no saturation effects are observed, strongly suggests that this peculiar behavior is caused by a subtle combination between the increasing presence of the *phonon-bottleneck process* (as the Nd^{3+} concentration increases) and the highly conducting metallic surface of this TI material.

Finally, we conclude that the *phonon-bottleneck process* allows the observation of several striking features on the Nd^{3+} ESR metallic linshape behavior within a skin depth of $\delta \approx 15$ μm in YBiPt, supporting the 3DTI character of this compound. We argue that the *phonon-bottleneck process* allowed the formation of *long life time phonons reservoir* where these phonons, via SO interaction, couple to highly mobile Dirac *ce* at the Fermi level that, finally, deliver the microwave energy absorbed at resonance by the Nd^{3+} ions to the thermal bath. We have also mentioned that electromagnetically excited electrons across the Fermi level at the Dirac cones by our low energy microwave photons may contribute to facilitate the observation of the diffusive effect of the Nd^{3+} ESR lineshape in $Y_{1-x}Nd_xBiPt$, although this contribution may not be so relevant due to our experimental configuration.

Acknowledgments

This work was supported by the auspices of FAPESP (Grant Nos. 2006/60440-0, 2007/50986-0, 2011/01564-0, 2012/05903-6), CNPq, FINEP and CAPES (Brazil), and NSF (DMR-0801253) (USA).

[1] X.-L. Qi and S.-C. Zhang, Phys. Today **63**, 33 (2010).
[2] M. Z. Hasan and C. L. Kane, Rev. Mod. Phys. **82**, 3045 (2010).
[3] J. E. Moore, Nature (London) **464**, 194 (2010).
[4] J. E. Moore and L. Balents, Phys. Rev. B **75**, 121306 (2007).
[5] L. Fu, C. L. Kane, and E. J. Mele, Phys. Rev. Lett. **98**, 106803(2007).
[6] R. Roy, Phys. Rev. B **79**, 195322 (2009).
[7] B. A. Bernevig, T. L. Hughes, and S.-C. Zhang, Science **314**, 1757 (2006).
[8] M. Konig, S. Wiedmann, C. Brune, A. Roth, H. Buhmann, L. W. Molenkamp, X.-L. Qi and S.-Q. Zhang, Science **318**, 766 (2007).
[9] L. Fu and C. L. Kane, Phys. Rev. B **76**, 045302 (2007).
[10] D. Hsieh, D. Quian, L. Wray, Y. Xia, Y. Hor, R. J. Cava and M. Z. Hasan, Nature (London) **452**, 970 (2008).
[11] H. Zhang et al., Nat. Phys. **5**, 438 (2009).
[12] Y. Xia et al., Nat. Phys. **5**, 398 (2009).
[13] Y. L. Chen et al., Science **325**, 178 (2009).
[14] M. Dzero, K. Sun, V. Galitski and P. Coleman, Phys. Rev. Lett. **104**, (2010).

[15] D. J. Kim, T. Grant and Z. Fisk, Phys. Rev. Lett. **109**, 096601 (2012).

[16] M. Neupane, N. Alidoust, S.-Y. Xu, T. Kondo, Y. Ishida, D. J. Kim, Chang Liu, I. Belopolski, Y. J. Jo, T.-R. Chang, H.-T. Jeng, T. Durakiewicz, L. Balicas, H. Lin, A. Bansil, S. Shin, Z. Fisk and M. Z. Hasan, Nat. Commun. **4**, 2991 (2013).

[17] D. J. Kim, J. Xia and Z. Fisk, Nat. Mater. advance online publication (2014).

[18] D. Culcer, Pysica E **44**, 860 (2012).

[19] X.-L. Qi and S.-C. Zhang, Rev. Mod. Phys. **83**, 1057 (2011).

[20] N. P. Butch, P. Syers, K. Kirshenbaum, A. P. Hope, and J. Paglione, Phys. Rev. B **84**, 220504(R) (2011).

[21] For a review, see Non-Centrosymmetric Superconductors, edited by E. Bauer and M. Sigrist, Lecture Notes in Physics Vol.**847** (Springer, Berlin, 2012).

[22] S. Chadov, X.-L. Qi, J. Keubler, G. H. Fecher, C. Felser, and S. -C. Zhang, Nat. Mater. **9**, 541 (2010).

[23] H. Lin, L. A. Wray, Y. Xia, S. Xu, S. Jia, R. J. Cava, A. Bansil, and M. Z. Hasan, Nat. Mater. **9**, 546 (2010).

[24] A. P. Schnyder, P. M. R. Brydon, and C. Timm, Phys. Rev. B **85**, 024522 (2012).

[25] P. C. Canfield, J. D. Thompson, W. P. Beyermann, A. Lacerda, M. F. Hundley, E. Peterson, Z. Fisk, and H. R. Ott, J. Appl. Phys. **70**, 5800 (1991).

[26] E. Mun, Ph.D. thesis, Iowa State University, 2010.

[27] F. F. Tafti, Takenori Fujii, A. Juneau-Fecteau, S. Rene de Cotret, N. Doiron-Leyraud, Atsushi Asamitsu, and Louis Taillefer, Phys. Rev. B **87**, 184504 (2013).

[28] G. Goll, M. Marz, A. Hamann, T. Tomanic, K. Grube, T. Yoshino, and T. Takabatake, Physica B **403**, 1065 (2008).

[29] R. H. Taylor, Advances in Physics **24**, 6, 681 (1975).

[30] S. E. Barnes, Advances in Physics **30**, 6, 801-938 (1981).

[31] G. B. Martins, D. Rao, G. E. Barberis, C. Rettori, R. J. Duro, J. Sarrao, Z. Fisk, S. Oseroff, and J.D. Thompson, Phys. Rev. B **52**, 15062 (1995).

[32] P. G. Pagliuso, C. Rettori, M. E. Torelli, G. B. Martins, Z. Fisk, J. L. Sarrao, M. F. Hundley, and S. B. Oseroff, Phys. Rev. B **60**, 4176 (1999).

[33] P. C. Canfield and Z. Fisk, Philos. Mag. B **65**, 1117 (1992).

[34] G. Feher and A. F. Kip, Phys. Rev. **98**, 337 (1955).

[35] F. J. Dyson, Phys. Rev. **98**, 349 (1955).

[36] J. I. Kaplan, Phys. Rev. **115**, 575 (1959).

[37] G. E. Pake and E. M. Purcell, Phys. Rev. **74**, 1184 (1948).

[38] EPR of Transition Ions, A. Abragam and B. Bleaney, Clarendon Press, Oxford, 1970.

[39] Electron Spin Resonance, a Comprehensive Treatise on Experimental Techniques, pgs 705-717, Charles P. Poole, Jr., Interscience Publishers, John Wiley & Sons Inc., NY, London, Sidney, 1969.

[40] R. L. Orbach, Proceed. Roy. Soc. **264**, 458 (1961). Electron Spin Relaxation in Solids, K. J. Standley and R. A. Vaughan, Plenum Press, NY, 1969.

[41] C. Rettori, D. Davidov, R. Orbach and E. P. Chock, Phys. Rev. B **7**, 1 (1973); C. Rettori, S. B. Oseroff, D. Rao, P. G. Pagliuso, G. E. Barberis, J. Sarrao, Z. Fisk, and M. Hundley, Phys. Rev. B **55**, 1016 (1997).

[42] Z. Fisk, private communication.

[43] Principles of Magnetic Resonance, pgs. 148-156, Charles P. Slichter, Harper & Row, NY, Evanston, London, 1963.

[44] J. D. N. Cheeke, J. de Physique, Colloque C3, Supp.10, Tome **31**, 129 (1970).

[45] N. H. Lindner, G. Refael, and V. Galitski, Nature Physics **7**, 490 (2011).